Fuel 320 (2022) 123953

Contents lists available at ScienceDirect

Fuel

journal homepage: www.elsevier.com/locate/fuel

Full Length Article

Kaolinite-based zeolites synthesis and their application in CO_2 capture processes

J.A. Cecilia [a], E. Vilarrasa-García [b], R. Morales-Ospino [b], E. Finocchio [c], G. Busca [c], K. Sapag [d], J. Villarroel-Rocha [d], M. Bastos-Neto [b], D.C.S. Azevedo [b], E. Rodríguez-Castellón [a,*]

[a] Department of Inorganic Chemistry, Crystallography and Mineralogy, Universidad de Málaga, Campus de Teatinos, 29071 Málaga, Spain
[b] Department of Chemical Engineering, Grupo de Pesquisa em Separações por Adsorção, Universidade Federal do Ceará, Campus do Pici, 60455760 Fortaleza, CE, Brazil
[c] Università degli Studi di Genova, Dipartimento di Ingegneria Civile, Chimica e Ambientale (DICCA), Laboratorio di chimica delle superfici e catalisi, Via Opera Pia 15, 16145 Genova, Italy
[d] Laboratorio de Sólidos Porosos (LabSoP), INFAP-CONICET, Universidad Nacional de San Luis, Av. Ejército de los Andes 950, 5700 San Luis, Argentina

ARTICLE INFO

Keywords:
Kaolinite
Zeolite type A
Synthesis
Characterization
CO_2 adsorption

ABSTRACT

In light of the urgent need of reducing the atmospheric CO_2 emissions, the use of low-cost adsorbents, that exhibit a high affinity and CO_2 adsorption capacity, is a promising method from the economic and environmental point of view to separate CO_2 from the flue gas emitted from large sources of emissions like power-fueled plants. Clay minerals are low-cost raw materials with high availability all over planet and great versatility in the fields of adsorption and catalysis processes. The present study pretends to elucidate the link between the reaction conditions during the synthesis of the zeolite from kaolinite and its CO_2 adsorption capacity. For that purpose, the type A zeolite was synthesized via hydrothermal process in alkaline solution using metakaolinite as a starting material. The metakaolinite was obtained by calcination of kaolinite at 600 °C and some parameters such as temperature and synthesis time were modified to optimize the synthesis aiming for a high CO_2 adsorption capacity adsorbent. Synthesized materials were characterized by X-ray diffraction (XRD), Fourier Transform Infrared Spectroscopy (FTIR), N_2 adsorption–desorption at −196 °C and CO_2 adsorption at 0 °C (up to 10 bars) isotherms and Nuclear Magnetic Resonance of solids (NMR). In addition, the adsorption capacity of CO_2 was evaluated by means of CO_2 adsorption–desorption isotherms at 25 °C up to atmospheric pressure. The obtained results indicated that synthesized zeolite 4A can be successfully prepared from natural kaolinite (via metakaolinization) at 100 °C for 48 h under alkaline conditions, showing chemical and physical properties similar to that of the commercial 4A zeolite.

1. Introduction

CO_2 capture from large releasing sources like fossil-fueled power plants is currently a key target to reduce the anthropogenic emissions of CO_2. Unfortunately CO_2 emissions into the atmosphere have been increasing yearly, due to the high energy demand related to industrial development and the increase in the world's population [1], becoming a major environmental concern worldwide motivating both governments and the scientific community to take steps to mitigate the CO_2 emissions [2,3]. According to the International Energy Agency (IEA), the world's electricity demand is expected to grow by 70% between 2010 and 2035 with coal as main fuel source for its generation [4].

Among the currently available technological pathways to capture CO_2 namely oxy-fuel combustion, pre-combustion capture, and post-combustion capture [5], the latter is the only route that can be easily retrofitted to the existing power plants [6]. Several processes including absorption, adsorption, membrane and cryogenics have been proposed to separate CO_2 from the flue gas [7,8]. Although CO_2 capture by adsorption processes using solid sorbents have shown many advantages [9] like no by-product generation such as wastewater as in conventional absorption processes [8], its commercial application requires further studies for its consolidation.

In an attempt to reduce the cost of CO_2 separation from flue gas, during the past few years several research groups have been engaged in the search and development of cost-effective, environmentally friendly and sustainable starting materials for the production of adsorbents for

* Corresponding author.
E-mail address: castellon@uma.es (E. Rodríguez-Castellón).

https://doi.org/10.1016/j.fuel.2022.123953
Received 28 December 2021; Received in revised form 18 March 2022; Accepted 20 March 2022
Available online 30 March 2022

CO_2 capture such as zeolites [10]. Zeolites are considered benchmark adsorbents for CO_2 capture from post combustion gas streams due to their favorable adsorption kinetics and high adsorption capacity at mild operating conditions (0–100 °C, 0.1–1 bar CO_2) [11]. Clay minerals are interesting precursors for the production of zeolites given their abundance and relatively low cost [12]. With a molar ratio of Si/Al almost equal to 1, kaolin clay is an ideal raw material for preparing type A zeolites [13]. Kaolinite mineral is a layered aluminosilicate of the phyllosilicate group having the chemical formula $Al_4Si_4O_{10}(OH)_8$ [14], may be regarded as a cheap natural source against conventional commercial process employing pure chemical reagents such as sodium silicate and sodium aluminate [15]. The transformation of kaolinite into zeolites comprises basically two steps: the activation of the kaolinite by its conversion into metakaolinite via calcination and the hydrothermal treatment of the metakaolinite in aqueous alkali solution to obtain the zeolites [10,16].

Rios et al. [17] studied two experimental routes to obtain zeolites from kaolinite: conventional hydrothermal treatment and alkaline fusion (at 600 °C) prior to hydrothermal reaction. Their results concluded that by using the first method, a mixture of different zeotypes was produced (e.g., sodalite and cancrinite) probably due to the instability of an intermediate zeolite LTA, whereas by the fusion method, kaolinite conversion into pure zeolite LTA was promoted, though its structural and morphological properties relied strongly on the aging conditions during the synthesis. Ayele et al. [18] also compared two synthesis routes to obtain zeolite type A using low grade kaolin: the conventional hydrothermal synthesis vs. alkali fusion followed by hydrothermal treatment. Different from the work of Rios et al. [17], their synthesis process always included the metakaolinization of the kaolin at 600 °C (during 3 h for the conventional method and 1 h with 1.5 g of NaOH for the alkali fusion method). They concluded that the alkali fusion method was more advantageous once it produces good quality zeolite A without the need to purify the raw kaolin. On the other hand, Wang et al. [19] reported the synthesis of zeolite type A by means of new method consisting of a hydrothermal reaction with an alkaline pretreatment followed by acid dissolution avoiding the conventional calcination at high temperatures. Their experiments indicated that by using this synthesis route, the impurities from the raw material are removed or transformed into the chemical target products (Si and Al) leading to a high purity zeolite A. Other works have reported conventional hydrothermal synthesis routes using different experimental conditions: Belviso et al. [20] synthesized both type A and X zeolites from kaolinite at low temperatures (between 25 and 60 °C) through hydrothermal activation during 96 h and established that the chemical composition of the starting material might be determinant in the type and the amount of zeolites formed, whereas Pereira et al. [21] studied the adsorption of cationic dyes such as methylene blue or safranine on synthesized zeolite 4A. The synthesized material was obtained after alkali treatment of metakaolinite, by calcination at 600 °C, with NaOH at 80 °C for 24 h. Most recently Wang et al. [22] estimated the CO_2 adsorption equilibrium of zeolites 4A prepared from low-grade kaolin following hydrothermal treatment. However, the CO_2 adsorption isotherms were carried out at high pressures (up to 45 bars), a pressure range far from post-combustion scenario carbon capture. The present work describes the synthesis of zeolite type A from a hydrothermal process in basic medium employing kaolinite as a starting material. In this study, several parameters such as temperature and reaction time were varied to assess the relationship between the formation conditions of the zeolite and its CO_2 adsorption uptake at mild conditions. Furthermore, with a view to its application in the flue gas separation, the nature of the interactions between CO_2 and the materials synthesized under dry and wet conditions was also analyzed.

2. Characterization techniques

X-ray powder diffraction patterns (XRD) were collected on an X'Pert Pro MPD automated diffractometer equipped with a Ge (111) primary monochromator (strictly monochromatic Cu-Kα radiation source, λ = 1.5406 Å) and an X'Celerator detector (Real Time Multiple Strip) with 128 Si aligned detectors.

The textural properties were evaluated from N_2 adsorption–desorption isotherms at −196 °C as determined by an automatic ASAP 2020 system supplied by Micromeritics®. Prior to the measurements, all samples were outgassed overnight at 300 °C and 10^{-4} mbar. The specific surface area was determined by the Brunauer-Emmett-Teller equation (BET) [23] using the adsorption data in the range of relative pressures at which conditions of linearity and considerations regarding the method were fulfilled. CO_2 adsorption isotherms at 0 °C up to 10 bars were measured with an automatic ASAP 2050 system supplied by Micromeritics®. The measurement error in both equipments (ASAP 2020 and ASAP 2050) is around 5–7% [24].The micropore volume (V_{mp}) was calculated from CO_2 adsorption isotherms at 0 °C by using the Dubinin-Radushkevich (DR) approach [25]. The error in the calculations of the micropore volume was obtained from the uncertainty in the Y-intercept to obtain the amount adsorbed on the monolayer, from the following equation (Equation (1)):

$$V_{mp,err} = V_{mp}(10^{Yerr} - 1) \quad (1)$$

where $V_{mp,err}$ [cm^3g^{-1}] is the calculated error, V_{mp} [cm^3g^{-1}] is de micropore volume obtained for DR method and Y_{err} is the error of the Y-intercept.

The FTIR spectra were collected in a Varian 3100 Fourier Transform Infrared (FTIR) spectrometer equipped with a Diffuse Reflectance Infrared Fourier Transform (DRIFT) cell. The interferograms consisted of 200 scans, and the spectra were collected using a KBr spectrum as background. For each analysis, about 50 mg of sample was mixed with KBr in a weight ratio of 1:9 and then the spectrum was collected.

To investigate the characteristic bonds involved in the adsorption of CO_2, N_2 and H_2O on zeolite synthesized from kaolinite and commercial zeolite, infrared absorbance spectra were collected during the exposure of the adsorbents to such gases. Spectra were collected in a FT IR Instrument Nicolet 380 spectrometer, which displays a DTGS detector and OMNIC software. The interferograms and spectra consisted of 200 scans. For each experiment, about 20 mg of pure powder pressed disks were outgassed in vacuum at 400 °C for 3 h in the IR cell and then the sample was cooled to room temperature. In the next step, the sample was putted in contact with CO_2 at two pressures (73 torr and 2 torr) and then the sample was outgassed at room temperature and several temperatures (150, 200 and 300 °C). For the coadsorption studies, N_2 or $H_2O_{(v)}$ were adsorbed prior to the CO_2 adsorption in the IR cell until the spectra did not suffer any changes. All spectra shown in this work were subtracted with respect to their respective spectrum after their activation and outgassing with He at 300 °C and their subsequent cooling to room temperature.

The ^{29}Si and ^{27}Al MAS NMR spectra were recorded using a Bruker AVIII HD 600 NMR spectrometer (with a field strength of 14.1 T) at 156.4 MHz with a 2.5 mm triple-resonance DVT probe that used zirconia rotors at the spinning rates of 15 kHz (^{29}Si) and 20 kHz (^{27}Al). The ^{29}Si experiments were performed with proton decoupling (cw (continuous wave) sequence) by applying a single pulse (π/2), an excitation pulse of 5 μs, and a 60 s relaxation delay to obtain 10,800 scans. The ^{27}Al experiments were also performed with proton decoupling (cw sequence) by applying a single pulse (π/12), an excitation pulse of 1 μs, and a 5 s relaxation delay to obtain 200 scans. The chemical shifts were referenced to as an external solution of tetramethylsilane and to an external solution of 1 M of $Al(NO_3)_3$ for ^{29}Si and ^{27}Al, respectively.

2.1. CO_2 adsorption measurements

CO_2 adsorption–desorption isotherms at 25 °C up to atmospheric pressure were measured using a Micromeritics ASAP 2020 Analyzer (i.

e., volumetrically equipment). Prior to the measurements, samples were outgassed at 300 °C and 10^{-4} mbar until full regeneration.

2.2. Equilibrium models

The Toth equation [26] is an empirical equation also employed to fit experimental adsorption data. The advantage of this model respect to the Sips equation is that at low pressures, Toth equation (Equation (2)) reduces to Henrýs law. The Toth equation can be written as follows:

$$q = \frac{q_m bP}{\left[1 + (bP)^t\right]^{1/t}} \tag{2}$$

where q [mmolg^{-1}] is the adsorbed amount per mass of adsorbent with q_m [mmolg^{-1}] as the maximum concentration, b [mmHg^{-1}] is known as the affinity parameter, P [mmHg] is the system pressure and t is the heterogeneity parameter. When t is equal to 1, Toth equation reduces to Langmuir model and the surface is considered as homogenous.

To estimate the accuracy of each fit, the Average Relative Error (ARE) (Eq. (3)), which is based on the relative difference between the experimental and estimated adsorbed amount, was used:

$$ARE(\%) = \frac{1}{N_T} \sum_{i=1}^{N_T} \frac{\left|q_{i,exp} - q_{i,est}\right|}{q_{i,exp}} * 100 \tag{3}$$

where N_T is the number of the data points, and $q_{i,\text{exp}}$ and $q_{i,est}$ are the experimental and estimated amounts of CO_2 adsorbed, respectively.

3. Materials synthesis

The material used for the synthesis of zeolites was a conventional kaolinite, a silicon and aluminum rich mineral clay. Kaolinite was subjected to thermal treatment at 600 °C for 120 min, in a furnace for complete transformation of crystalline kaolinite to amorphous metakaolinite, by means of dehydroxylation. Then, zeolite 4A was synthesized from metakaolinite by hydrothermal reaction, mixing metakaolinite with sodium hydroxide under different conditions of reaction time and temperature. Thus, a series of materials was obtained varying the synthesis temperature between 60 and 120 °C and the aging time between 6 and 168 h. For each experiment, 1 g of metakaolinite was treated with 40 mL de NaOH 2 M. The obtained samples were washed with distilled water filtered. The solid materials were dried in an oven at 60 °C overnight.

4. Results and discussion

4.1. Characterization

The powder X-ray diffraction pattern for kaolinite, metakaolinite, commercial zeolite 4A and synthesized materials are shown in Fig. 1(A) and Fig. 1(B). From these data, it can be observed how kaolinite displays high-grade of crystallinity. Besides kaolinite, the starting raw clay also displays small proportion of silica. The thermal treatment of the kaolinite at 600 °C leads to metakaolinite, which exhibits a clear amorphization in such a way the diffraction peaks ascribed to quartz are only observed.

The hydrothermal treatment under basic conditions always lead to diffraction peaks, which resemble to the commercial zeolite 4A. The synthesized samples show reflections located at 2θ = 7.2, 10.1, 12.5, 16.2, 21.7, 24, 26, 27.1, 30, 30.9, 32.7 and 34.4°, typical of a type A zeolite. These reflections are related to (200), (220), (222), (420), (600), (622), (640), (642), (694), (660), (842) and (664) [13,27]. As the aging time increases, the crystallinity of the synthesized materials also does so, reaching a maximum value for the synthesized sample at 100 °C/96 h, where the crystallinity is very close to that of commercial zeolite 4A. From this point on, the progressive amorphization of the sample is noticeable as seen in Fig. 1(A).

The synthesis temperature has also a relevant role on the crystallinity of the obtained samples, reaching a maximum at 100 °C/48 h. The sample synthesized at 120 °C for 48 h displays 30% of 4A commercial zeolite crystallinity, as observed in Fig. 2. These results are in accordance with Cui et al. [28].

Kaolinite, metakaolinite as well as zeolite synthesized at 100 °C during 48 h and commercial 4A zeolite were also characterized by FT-IR (Fig. 3). Between 3750 and 3500 cm^{-1}, kaolinite spectrum shows four bands. The band located at higher wavenumber (3692 cm^{-1}) is assigned to the presence of the in-phase symmetric stretching vibration mode while the band located at 3669 and 3650 cm^{-1} are attributed to out-of-plane stretching vibration modes. Finally, the band located about 3620 cm^{-1} is ascribed to the inner hydroxyl groups of kaolinite [29]. The region (1300–400 cm^{-1}) compiles Si–O stretching and bending as well as OH bending adsorption modes. In this region, it is noteworthy the presence of well-resolved bands located between 1120 and 1000 cm^{-1} assigned to Si-O stretching vibrations [30]. The band located about 936 and 910 cm^{-1} is assigned to Al_2OH bending bands of inner and surface OH groups [30]. The band located at 540 and 470 cm^{-1} are assigned to Si-O-Al and Si-O-Si bending vibrations, respectively [30]. The thermal treatment to form metakaolinite causes a modification of the FT-IR spectrum. Thus, it can be observed how the bands ascribed to –OH stretching modes disappear due to thermal at 600 °C promotes the dehydroxilation of kaolinite [31,32]. In the region between 1300 and

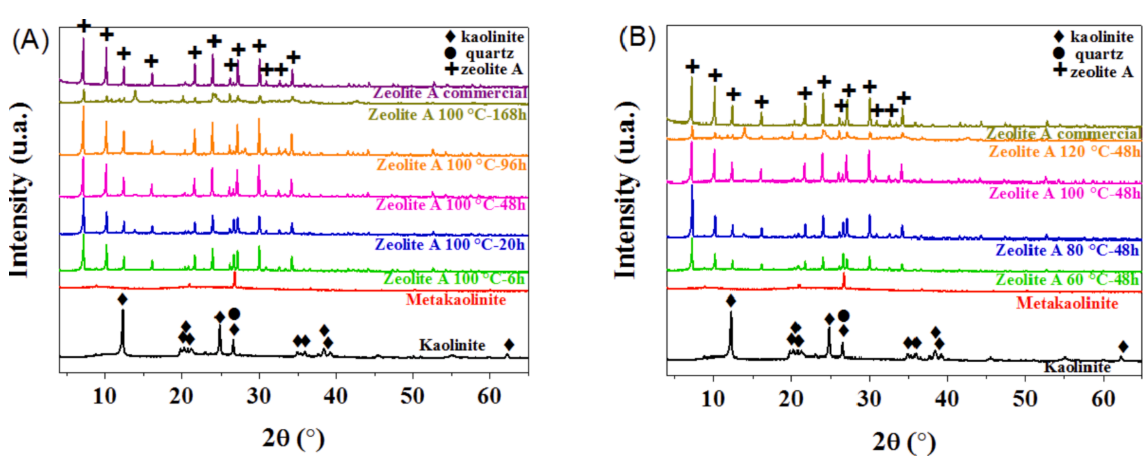

Fig. 1. X-ray diffraction patterns of kaolinite, metakaolinite and zeolites synthesized variyng (A) the aging time and (B) the synthesis temperature.

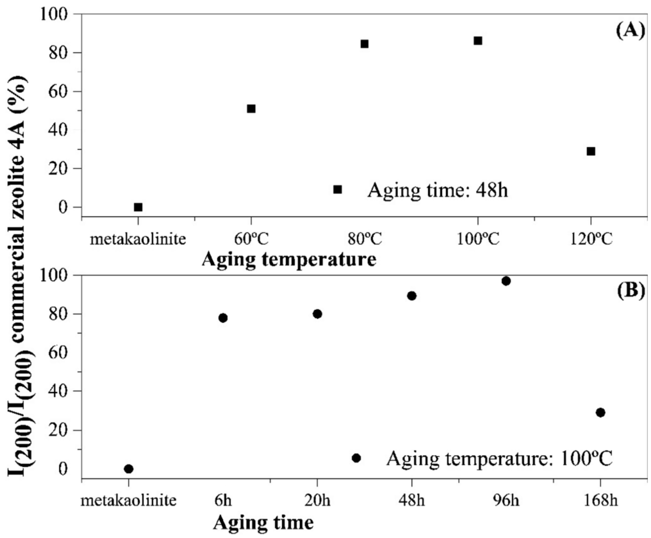

Fig. 2. Influence of (A) the aging time and (B) the aging temperature on the crystallinity of the obtained zeolites. The XRD intensities are calculated for the strongest reflections (200).

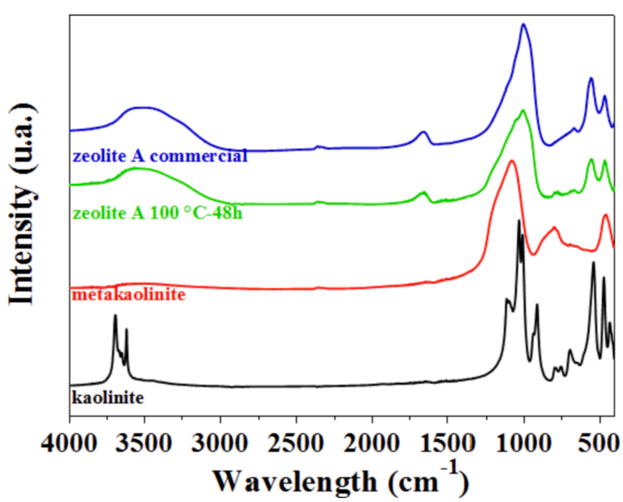

Fig. 3. FTIR spectra of kaolinite, metakaolinite, zeolite A synthesized from metakaolinite at 100 °C during 48 h and commercial zeolite 4A.

400 cm^{-1}, clear modifications can also be observed when metakaolinite is synthesized, emerging broad bands whose maxima are located at 1080, 795 and 460 cm^{-1} due to the amorphization after the thermal treatment [30]. Finally, the bands of zeolite A-type synthesized at 100 °C during 48 h are very similar to the commercial 4A zeolite ones. The bands located at around 1000, 550 and 460 cm^{-1} are assigned to Si-O stretching vibration mode, Si-O-Al and Si-O-Si bending vibrations [22]. In addition, the band located at 1650 cm^{-1} is related to interstitial bonded water and the broad band located between 3000 and 3500 cm^{-1} is attributed to intra- and inter-molecular hydrogen bonding [28,33]. The results of FTIR are in accordance with XRD, confirming that 4A zeolite has been appropriately synthesized from kaolinite under the studied conditions.

The ^{27}A1 and ^{29}Si nuclear magnetic resonance (NMR) of kaolinite, metakaolinite, synthesized zeolite at 100 °C during 48 h and commercial zeolite 4A are shown in Fig. 4. It can be seen in Fig. 4A that Al-species evolve from an octahedral environment (5 ppm) in the case of kaolinite [34] to a tetrahedral environment (60 ppm) when zeolite 4A is synthesized so Al-species enter into the coordinate Si-O network to form the framework $Si(OAl)_3(OSi)$ after the hydrothermal treatment [22,35–37].

In the ^{29}Si NMR spectrum of kaolinite (Fig. 4B), it can be observed a signal about −91 ppm. Previous authors have pointed out that this signal can be ascribed of overlapping SiO_4 tetrahedrons (three bridged oxygen atoms and one non-bridged oxygen) [34]. After the thermal treatment to obtain metakaolinite, the dehydroxilation of the kaolinite causes a decrease in the signals observed in its spectra due to an impoverish of the crystallinity [38]. The synthesis of the 4A zeolite causes a shift of the band to −89 ppm, which is assigned to Si atom in Q^4 (4Al) environment, which is typical of four-member ring and β-cage, suggesting that the obtaining sodium aluminosilicate displays a large amount of four-member ring and β-cage [35,36].

In order to study the textural properties of kaolinite, metakaolinite, zeolite A 100 °C/48 h and commercial 4A zeolite a first approximation was carried out analyzing their N_2 adsorption/desorption isotherms at −196 °C (Fig. S1). In all cases, it can be observed how the materials hardly adsorb at low relative pressure while the main N_2-adsorption takes place at high relative pressure. This fact should indicate that these materials lack of microporosity and the small porosity is attributed to the voids between adjacent particles. Considering that zeolites display excellent properties in the adsorption and separation processes it does not seem logical to obtain such low adsorption values. In this sense, the diffusional resistances of N_2 at −196 °C in the small pores of the type A zeolites at low pressures are very high. The pore width of type A zeolites is close to the molecular diameter of N_2 molecule, making it difficult for N_2 molecules to access to the pore grid. This fact derives in a negligible BET surface area measurement, i.e. <15 $m^2.g^{-1}$ [39,40]. This experimental limitation makes unfeasible to characterize this kind of samples

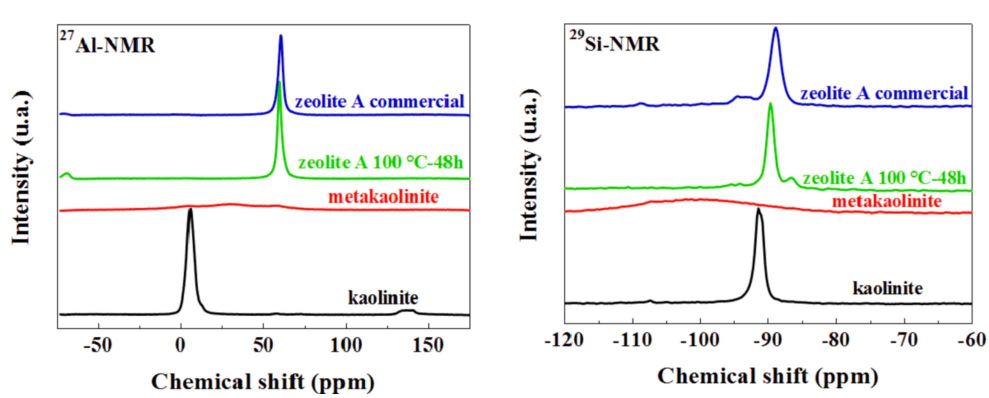

Fig. 4. ^{27}Al nuclear magnetic resonance (NMR) (left) and ^{29}Si NMR (right) spectra of kaolinite, me takaolinite, synthesized zeolite at 100 °C during 48 h and commercial zeolite 4A.

by N_2 adsorption at −196 °C.

In order to analyze the textural properties of these materials, it is necessary to draw on to CO_2 adsorption isotherms at 0 °C. Thus, CO_2 adsorption isotherms were collected up to 10 bar and 0 °C and the results are plotted in Figure S2. Note that as the temperature increases, textural properties improve and approach to commercial A zeolite ones, reaching a maximum micropore volume of 0.20 ± 0.03 cm^3g^{-1} for the zeolite synthesized at 100 °C for 96 h, which is very close to that obtained for the commercial 4A zeolite, as observed in Table 1. At 120 °C, the collapse of the zeolitic structure takes place and the amount of CO_2 adsorbed drops drastically. The drop in the textural properties and crystallinity observed at 120 °C may be related with the formation of separated SiO_2 or Al_2O_3 phases due to the rapid nucleation. From the obtained data, it can be observed how the porosity of the zeolites is directly related to the crystallinity of the zeolite (Figs. 1 and 2). In any case, micropore volume values of all zeolites are much higher than those achieved by raw kaolinite and metakaolinite.

Given these results, the sample synthesized at 100 °C for 48 h was selected to continue the characterization due to it reached the highest crystallinity index (respect to commercial 4A zeolite) in the shortest synthesis time.

4.2. Equilibrium adsorption measurements

CO_2 adsorption measurements at 25 °C up to 1 bar were carried out on ASAP 2020 (Micromeritics). In the first time, the CO_2 adsorption capacity of kaolinite and metakaolinite was evaluated. It can be observed how CO_2 uptake is very low for both materials, reaching an adsorption value of 0.06 and 0.04 mmol/g for kaolinite and metakaolinite at 25 °C and 1 bar of pressure. The synthesis of zeolites leads to adsorbents with a notable CO_2 adsorption capacity in comparison to the starting materials (kaolinite and metakolinite). In order to optimize the synthetic parameters to obtain adsorbents with high CO_2 adsorption capacity, it was fixed the synthesis temperature (100 °C), taking into account that type A zeolites are commonly synthesized from clay minerals at temperatures in the range of 90–200 °C, while the aging temperature was modified from 6 h to 168 h [10] (Fig. 5A). The study of the CO_2 adsorption data at 1 bar reveals that the increase of the aging time improves the adsorption capacity, reaching a higher adsorption capacity for those samples aged at 48 and 96 h with a CO_2 uptake of 2.48 and 2.53 mmol/g at 25 °C, respectively. These values are very close and fall within the measurement error. It is noticeable that his value is very close to that observed for the commercial 4A zeolite, where a CO_2 adsorption of 2.72 mmol/g was reached at 1 bar of pressure and 25 °C.

Then, in a second study, several zeolites were synthesized from metakaolinite at different temperatures 60–120 °C, maintaining the aging temperature for 48 h (Fig. 5B). The modification of the temperature seems to be a key parameter in the adsorption capacity since CO_2 adsorption improves notably in comparison to kaolinite and metakaolinite. These data show how CO_2 uptake rises, according to the aging temperature increases from 0.80 mmol/g when A zeolite was aged at 60 °C to 2.48 mmol/g for the zeolite aged at 100 °C. The use of higher aging temperature (i.e. 120 °C) drastically worsens the CO_2 adsorption capacity, reaching a value of only 0.75 mmol/g at 25 °C and a pressure of 1 bar.

Table 1
Micropore volume determined by Dubinin Radushkevich method.

Sample	V_{mp} (cm^3 g^{-1})	Sample	V_{mp} (cm^3 g^{-1})
Zeolite 100 °C 6 h	0.10 ± 0.02	Zeolite 60 °C 48 h	0.06 ± 0.01
Zeolite 100 °C 20 h	0.13 ± 0.02	Zeolite 80 °C 48 h	0.14 ± 0.03
Zeolite 100 °C 48 h	0.19 ± 0.03	Zeolite 100 °C 48 h	0.19 ± 0.03
Zeolite 100 °C 96 h	0.20 ± 0.03	Zeolite 120 °C 48 h	0.04 ± 0.01
Zeolite 100 °C 168 h	0.11 ± 0.03	Commercial	0.22 ± 0.03
Kaolinite	0.01 ± 0.00	Metakaolinite	0.00 ± 0.00

The development of the micropore network and the increase of crystallinity as the aging temperature increases improve the CO_2 adsorption capacity, reaching a maximum at 100 °C close to that of commercial zeolite. From this aging temperature, the kinetics of crystal nucleation leads to phase segregation, causing a decrease in the CO_2 adsorption capacity. Duan and coworkers [41], synthesized zeolite from acid-pretreated kaolinite and they found 170 °C as the optimal aging temperature to improve crystallinity. In our work, from the basic treatment of kaolinite we have significantly reduced this aging temperature.

On the other hand, it is also noticeable that all zeolites display isotherm profiles, which are typical of microporous materials, namely, the quantity of CO_2 adsorbed increases abruptly with the increase on the equilibrium pressure in the low-pressure range, and smoothly at higher pressures. This type of isotherm is related to type-I isotherm according to International Unit Pure and Applied Chemistry (IUPAC) classification [42] and is characteristic of adsorption in monolayer. In fact, it can be observed a clear relation between of the CO_2 adsorption capacity and the micropore volume since those adsorbents with higher CO_2 uptake are also those materials with higher microporosity (Fig. 6A).

The CO_2 adsorption isotherms for the synthesized zeolites and commercial 4A zeolite were well fitted to Toth equilibrium equation. This adsorption model assumes that the adsorption exclusively takes place with sub-monolayer coverage.

The CO_2 adsorption isotherms for kaolinite and metakaolinite were not fitted to any model due to the amount of CO_2 adsorbed for both materials were negligible in comparison to the synthesized and commercial zeolites. The fitting parameters are collected in Table 2.

In general terms, Toth equation well fits the experimental data, showing low values of average relative errors. Another parameter that must be considered is parameter b, which defines the affinity between adsorbate and adsorbent. From these data, those adsorbents that interact strongest with CO_2 molecules can be predicted. It can be observed that the adsorption is directly related to b-parameter and, in turn, these values are also related to microporosity. These data infer that those adsorbents with a higher microporosity favor a greater CO_2 capture capacity due to a strong interaction between these micropores and the CO_2 molecules due to their significant quadrupole moment (Fig. 6B). Then, controlling the crystallinity through temperature and aging time, materials with microporosity similar to zeolite 4A are obtained, reaching CO_2 adsorption capacities similar to the commercial material.

4.3. FTIR adsorption measurements

DRIFT subtraction spectra for CO_2 adsorption at 73 and 2 torr (25 °C) on commercial 4A zeolite and sample synthesized from kaolinite at 100 °C and 48 h are plotted in Fig. 7A-C. The spectra were collected after outgassing in situ at 300 °C under He flow for 3 h. In the case of the raw kaolinite, the subtracted spectra show how CO_2 adsorption is negligible, which agree with those data obtained from the CO_2 isotherms at 1 bar and 25 °C (Fig. 5). With regard to the subtracted spectra or synthesized and commercial zeolite, both spectra are very similar between them. After CO_2 dosing (73 torr) appears two bands. The strong band located at 2350 cm^{-1} is assigned to CO_2 physisorbed (OCO asymmetric stretching). This wavenumber value is higher than that observed for CO_2-gaseous, suggesting that the coordination of the CO_2 molecules with the Lewis sites of the zeolite takes place from the O-atoms of the zeolite so the coordination must generate a linear structure [43].

At lower wavenumber values, it can be observed several bands located at 1678, 1649 and 1620 cm^{-1} after the outgassing so this set of bands must be ascribed to CO_2-chemisorbed in the form of bridging or bidentate carbonate species [44,45]. In this sense, previous authors have reported that the bands at higher wavenumber values are assigned to the split asymmetric stretching mode of the carbonate ion while the band located at lower wavenumber values is attributed to the split asymmetric stretching mode although this band could be masked by the

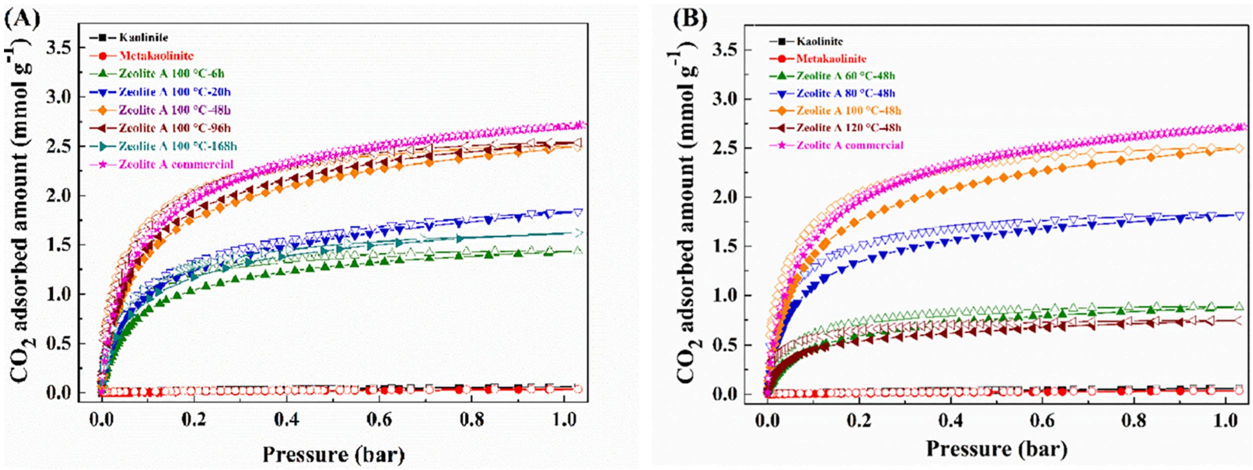

Fig. 5. CO_2 adsorption/desorption isotherms at 25 °C for kaolinite, metakaolinite, commercial 4A zeolite and (A) zeolites synthesized at different aging time (96–168 h) keeping constant the aging temperature (100 °C) and (B) zeolites synthesized at different aging temperature (60–120 °C) keeping constant the aging time (48 h).

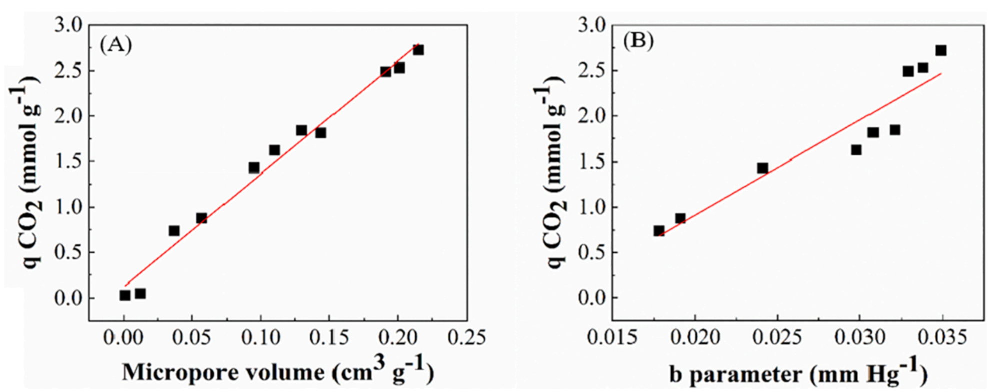

Fig. 6. Relationship between the CO_2 adsorption capacity (at 25 °C and 1 bar) and (A) microporosity of the adsorbents and (B) b-parameter estimated by the Toth equation.

Table 2
Toth model parameters for CO_2 adsorption on zeolite synthesized at different aging time.

Sample	q_m	b	t	ARE (%)
Zeolite 100 °C 6 h	1.682	0.0241	0.709	1.893
Zeolite 100 °C 20 h	2.652	0.0321	0.477	2.361
Zeolite 100 °C 48 h	3.075	0.0329	0.632	2.521
Zeolite 100 °C 96 h	3.259	0.0338	0.573	2.711
Zeolite 100 °C 168 h	2.011	0.0298	0.619	0.473
Sample	q_m	b	T	ARE (%)
Zeolite 60 °C 48 h	1.097	0.0191	0.641	2.011
Zeolite 80 °C 48 h	2.156	0.0308	0.641	0.727
Zeolite 100 °C 48 h	3.075	0.0329	0.632	2.521
Zeolite 120 °C 48 h	0.813	0.0178	0.675	1.483
Commercial	3.398	0.0349	0.605	0.223

*q_m:[$mmolg^{-1}$], b:[$mmHg^{-1}$], t: [dimensionless].
ARE: average relative error.

skeletal modes. The small band located about 1430 cm^{-1} is assigned to the presence of carbonate species in the form of monodentate, and bidentate or bridging.

The band located about 1380 cm^{-1} is ascribed to the symmetric stretching mode of CO_2 molecules adsorbed linearly [43,45].

After the thermal treatment, it can be observed how the band located about 2350 cm^{-1} disappears so, as was expected, physisorbed CO_2 is released at 150 °C. However, the bands ascribed to chemical interactions (1700–1600 cm^{-1}) by the formation of monodentate, bidentate or bridging carbonate-like species are still observed at this temperature, which confirms the stability of these carbonate species [43]. The decrease in the intensity of these bands as the temperature increases may be related with the higher proportion of bidentate carbonates over monodentate species. The FTIR bands related to CO_2 monodentate species remain constant up to 250 °C while the bands associated to CO_2-bidentate species decrease in intensity from 150 °C [46]. These results show that the CO_2 adsorption mechanism in both commercial zeolite and that synthesized from natural sources is the same.

As the CO_2-adsorption results of the zeolite synthesized at 100 °C and 48 h are very close to those obtained for the commercial zeolite, the next studies will be carried out for this synthesized zeolite. In order to evaluate the stability of this zeolite, several CO_2-adsorption cycles were evaluated by FTIR (Fig. 8). In all cycles, it can be observed the same bands with similar intensities, so it is expected that this zeolite maintain its structure and CO_2 uptake. It is noteworthy that the subtracted spectrum after the outgassing for 30 min shows that the band located at 2350 cm^{-1} is less intense than that observed in Fig. 8B. This indicates that the proportion of physisorbed-CO_2 is lower in this test probably due to slight modifications in the time of outgassing. However, similar trend is observed since CO_2 chemisorbed as monodentate, bidentate or bridging carbonate-species is strongly adsorbed requiring an increase of the temperature to promote its desorption and its reuse in the next cycle.

In the next FTIR studies, the zeolite synthesized at 100 °C and 48 h was undergone to a prior adsorption with some gases such as N_2 or H_2O

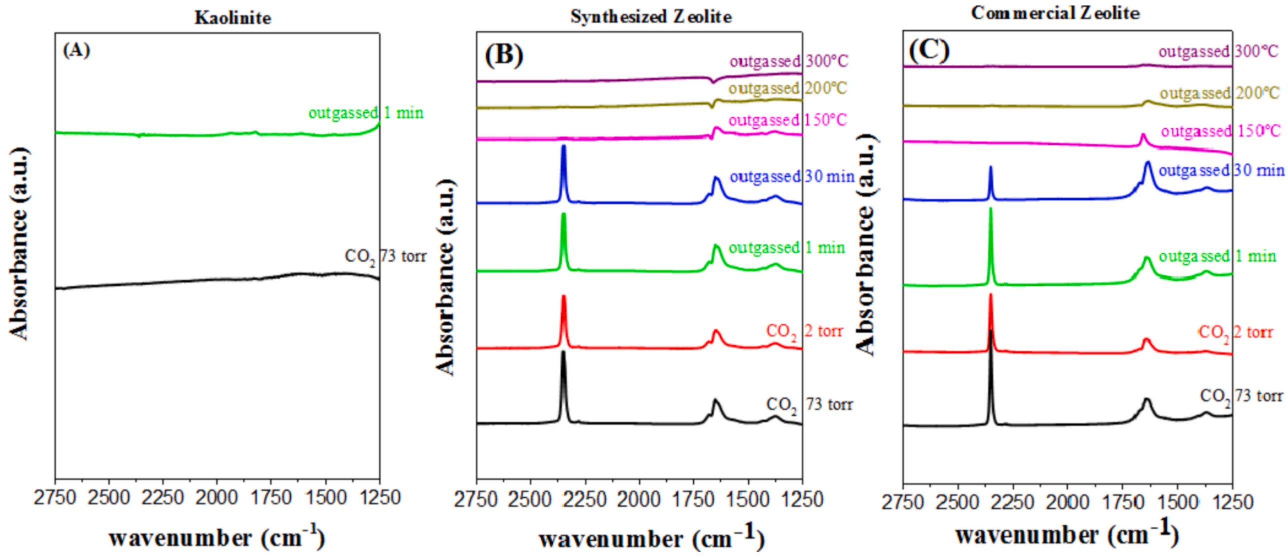

Fig. 7. DRIFT substraction spectra recorded for raw kaolinite (A) zeolite synthesized at 100 °C and 48 h (B) and commercial 4A zeolite after CO_2 adsorption at 20 °C, after outgassing (1 min and 30 min) and after heating at 150, 200 and 300 °C.

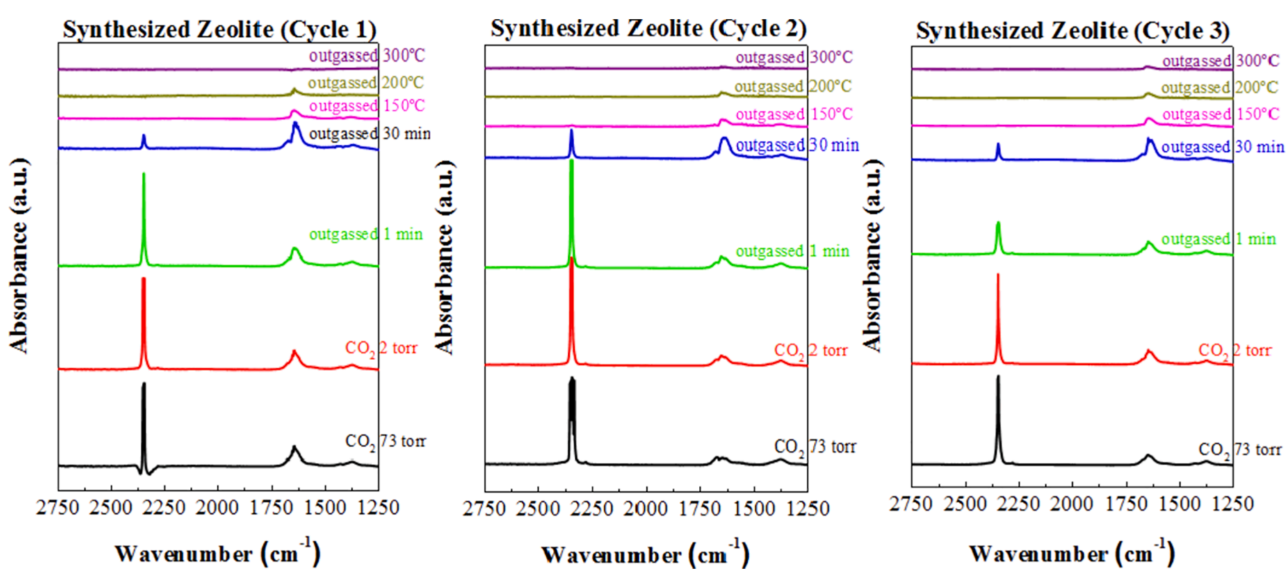

Fig. 8. DRIFT substraction spectra recorded for zeolite synthesized at 100 °C and 48 h (B) CO_2 adsorption at 20 °C, after outgassing (1 min and 30 min) and after heating at 150, 200 and 300 °C for three cycles.

and outgassed at room temperature and then this sample was treated with CO_2 (Fig. 9).

In the case of the sample treated with $CO_2 + N_2$ (Fig. 9A), the subtracted spectra do not reveal the presence of any band assigned to N_2-adsorption, which should appear about 2335 cm^{-1} as a consequence of N-N stretching mode of N_2 polarized by silanol groups [47] discarding physical or chemical interactions between the synthesized zeolite and N_2-molecules. On the other hand, the subtracted spectra also reveals that the pre-adsorption of N_2 hardly affect in the CO_2 adsorption. Similarly to that observed in Fig. 7 and Fig. 8, the subtracted spectra confirm the physical and chemical adsorption of CO_2 molecules. Between them, the physical sites (2350 cm^{-1}) disappear after the outgassing at 25 °C for 30 min. However, the CO_2 molecules that have been chemically adsorbed require higher temperatures for desorption. From these data, it can be concluded that this zeolite displays a selective adsorption for CO_2 molecules in such a way this adsorbent could be used for the capture of CO_2 molecules in flue gas. Fig. 9B displays the subtracted spectra of zeolite synthesized 100 °C and 48 h CO_2 saturated with H_2O(v) and then CO_2 was adsorbed at 25 °C. Note that under humid conditions, the bands located at lower wavenumber values, ascribed to formation of carbonate in the form of monodentate, bidentate or bridging species, are less intense than those in dry conditions (Fig. 7B) probably due to presence of traces H_2O in the zeolite. The high attraction of zeolites to adsorb water is given by the strong interactions with the Na^+-species of the zeolite forming a coordination sphere surrounding the alkali cation [48]. Specifically, the permanent dipole of the water molecule (1.87 D) causes strong interactions with the charges of the materials whose affinity for CO_2 is the result of its quadrupole moment [49]. Therefore, the presence of water molecules strongly affects the availability of chemisorption sites for CO_2. The intense band located at 2350 cm^{-1}, previously attributed to CO_2 physisorbed, remains after heating at 150 °C, being only removed when the temperature rises to 200 °C. This fact was not observed in dry conditions, where outgassing at room temperature was enough to remove CO_2 physisorbed. Under humid conditions, CO_2 may be adsorbed in adsorbed water in the cavities or as hydrogencarbonate ion on the surface. The difficulty in releasing the gas

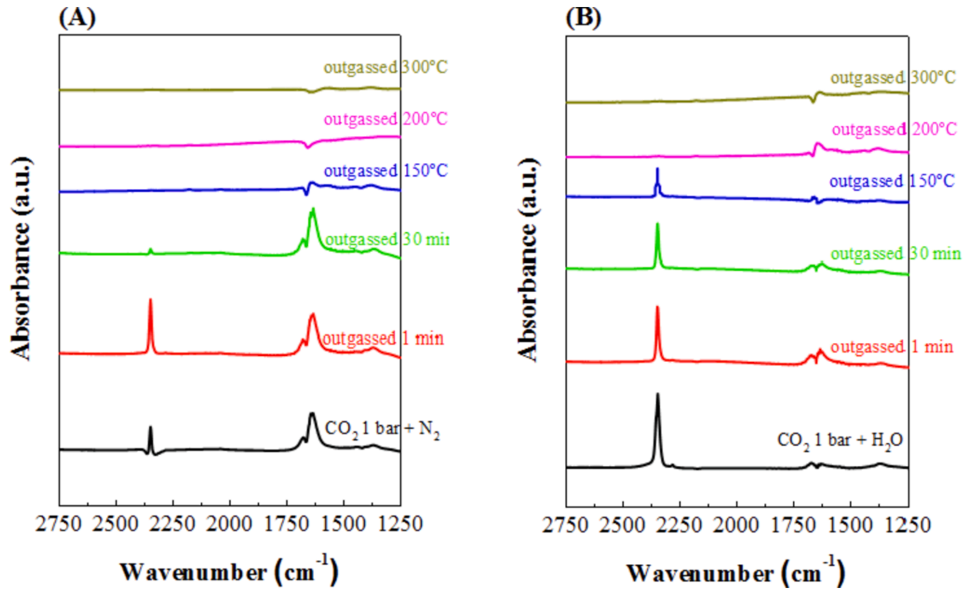

Fig. 9. DRIFT substraction spectra recorded for sample zeolite synthesized at 100 °C and 48 h after CO_2 and N_2 coadsorption at 25 °C (A) and CO_2 and H_2O coadsorption at 25 °C (B), after degassing (1 min and 30 min) and after heating at 150, 200 and 300 °C.

would be related to diffusional resistances of CO_2 for desorbing from the interior of the cavities occupied by water clusters, requiring an extra heat energy supply to desorb CO_2.

5. Conclusions

High crystallinity type A zeolite was successfully synthesized from natural kaolinite via two-step route. The two-step synthesis consisted in a thermal metakaolinization of kaolinite at 600 °C for 2 h and hydrothermal treatment. During the hydrothermal treatment, the influence of the aging time and the aging temperature were assessed by means of varying both parameters. The optimum synthesis was carried out at 100 °C during 48 h, obtaining a zeolite type A with almost 90% of crystallinity respect to the 4A commercial zeolite. In addition, ^{27}Al nuclear magnetic resonance confirmed the incorporation of Al atoms coordinated with Si-O network. CO_2 adsorption tests at 25 °C revealed that the synthesized zeolite under these conditions showed a very similar performance respect the commercial 4A zeolite, reaching 2.5 mmol g^{-1} at 25 °C and 1 bar. Under dry conditions, CO_2 is strongly adsorbed at room temperature probably with linear interaction CO_2–zeolite cations and non linear species formed as mono or bidentate carbonate. Under humid conditions, hydrogencarbonate is formed in zeolitic cavities and remains up to 150 °C, even at low CO_2 partial pressures. The presence of water, due to the high permanent dipole, decreases the relative intensity of the IR bands related to CO_2 chemisorbed but hinders the desorption of the physisorbed species. Therefore, we have shown that a material similar to zeolite 4A can be synthesized from natural kaolinite, reducing wastes and environmental impacts. This material presents stability in adsorption/desorption cycles and could be used in cyclic adsorption processes for separation of flue gases. We have also shown that in dry conditions, the physisorbed CO_2 is desorbed at mild temperatures while the presence of water hinders the desorption, requiring an extra input of energy to remove CO_2.

CRediT authorship contribution statement

J.A. Cecilia: Investigation, Writing – original draft, Validation. **E. Vilarrasa-García:** Investigation, Writing – original draft. **R. Morales-Ospino:** Investigation. **E. Finocchio:** Investigation. **G. Busca:** Conceptualization, Investigation. **K. Sapag:** Conceptualization, Validation. **J. Villarroel-Rocha:** Investigation. **M. Bastos-Neto:** Conceptualization, Validation, Writing – review & editing. **D.C.S. Azevedo:** Conceptualization, Validation, Supervision, Funding acquisition. **E. Rodríguez-Castellón:** Investigation, Validation, Supervision, Funding acquisition.

Declaration of Competing Interest

The authors declare the following financial interests/personal relationships which may be considered as potential competing interests: Enrique Rodriguez-Castellon reports financial support was provided by Ministry of Science, Innovation and Universities. Enrique Rodriguez-Castellon reports financial support was provided by Government of Andalusia Ministry of Economy Science Innovation and Employment. Diana C.S. Azevedo reports financial support was provided by Conselho Nacional de Desenvolvimento Científico e Tecnológico. Diana C.S. Azevedo reports financial support was provided by Coordination of Higher Education Personnel Improvement.

Acknowledgements

This research was funded by the Ministry of Science, Innovation and Universities (Spain), Grant Nos. RTI2018-099668-B-C22 and project UMA18-FEDERJA-126 and P20_00375 of Junta de Andalucía (Spain) and FEDER funds (European Union). We also thank to Conselho Nacional de Desenvolvimento Científico e Tecnológico (CNPq, Ministry of Science and Technology, Brazil) and CAPES/PrInt (Project 88887.311867/2018-00) (Ministry of Education, Brazil) for financial support.

Appendix A. Supplementary data

Supplementary data to this article can be found online at https://doi.org/10.1016/j.fuel.2022.123953.

References

[1] Yeh J-C, Liao C-H. Impact of population and economic growth on carbon emissions in Taiwan using an analytic tool STIRPAT. Sustainable Environ Res 2017;27(1): 41–8. https://doi.org/10.1016/j.serj.2016.10.001.

[2] Nie L, Mu Y, Jin J, Chen J, Mi J. Recent developments and consideration issues in solid adsorbents for CO_2 capture from flue gas. Chin J Chem Eng 2018;26(11): 2303–17. https://doi.org/10.1016/j.cjche.2018.07.012.

[3] Liang Z, Fu K, Idem R, Tontiwachwuthikul P. Review on current advances, future challenges and consideration issues for post-combustion CO_2 capture using amine-

based absorbents. Chin J Chem Eng 2016;24(2):278–88. https://doi.org/10.1016/j.cjche.2015.06.013.
[4] Salazar Duarte G, Schürer B, Voss C, Bathen D. Adsorptive separation of CO_2 from flue gas by temperature swing adsorption processes. ChemBioEng Rev 2017;4(5):277–88. https://doi.org/10.1002/cben.201600029.
[5] Figueroa JD, Fout T, Plasynski S, Mcilvried H, Srivastava RD. Advances in CO_2 capture technology—The U.S. Department of Energy's Carbon Sequestration Program. Int J Greenhouse Gas Control 2008;2(1):9–20. https://doi.org/10.1016/s1750-5836(07)00094-1.
[6] Tan Y, Nookuea W, Li H, Thorin E, Yan J. Property impacts on Carbon Capture and Storage (CCS) processes: a review. Energy Convers Manage 2016;118:204–22. https://doi.org/10.1016/j.enconman.2016.03.079.
[7] Olajire AA. CO_2 capture and separation technologies for end-of-pipe applications – a review. Energy 2010;35(6):2610–28. https://doi.org/10.1016/j.energy.2010.02.030.
[8] Mondal MK, Balsora HK, Varshney P. Progress and trends in CO_2 capture/separation technologies: a review. Energy 2012;46(1):431–41. https://doi.org/10.1016/j.energy.2012.08.006.
[9] Shi Y, Liu Q, He Y. CO_2 capture using solid sorbents. In: Handbook of climate change mitigation and adaptation. New York, NY: Springer New York; 2014. p. 1–56.
[10] Abdullahi T, Harun Z, Othman MHD. A review on sustainable synthesis of zeolite from kaolinite resources via hydrothermal process. Adv Powder Technol 2017;28(8):1827–40. https://doi.org/10.1016/j.apt.2017.04.028.
[11] Spigarelli BP, Kawatra SK. Opportunities and challenges in carbon dioxide capture. J CO_2 Utiliz 2013;1:69–87. https://doi.org/10.1016/j.jcou.2013.03.002.
[12] Johnson EBG, Arshad SE. Hydrothermally synthesized zeolites based on kaolinite: a review. Appl Clay Sci 2014;97–98:215–21. https://doi.org/10.1016/j.clay.2014.06.005.
[13] Miao Q, Zhou Z, Yang J, Lu J, Yan S, Wang J. Synthesis of NaA zeolite from kaolin source. Front Chem Eng China 2009;3(1):8–11. https://doi.org/10.1007/s11705-009-0094-8.
[14] Bajpai P. Chapter 3 - Pulp and paper chemicals. In: Pulp and paper industry. Amsterdam: Elsevier; 2015. p. 25–273.
[15] Youssef H, Ibrahim D, Komarneni S. Microwave-assisted versus conventional synthesis of zeolite A from metakaolinite. Microporous Mesoporous Mater 2008;115(3):527–34. https://doi.org/10.1016/j.micromeso.2008.02.030.
[16] Rocha J, Klinowski J, Adams JM. Synthesis of zeolite Na-A from metakaolinite revisited. J Chem Soc, Faraday Trans 1991;87(18):3091–7. https://doi.org/10.1039/FT9918703091.
[17] Rios C, Williams C, Fullen M. Nucleation and growth history of zeolite LTA synthesized from kaolinite by two different methods. Appl Clay Sci 2009;42(3–4):446–54. https://doi.org/10.1016/j.clay.2008.05.006.
[18] Ayele L, Pérez-Pariente J, Chebude Y, Díaz I. Conventional versus alkali fusion synthesis of zeolite A from low grade kaolin. Appl Clay Sci 2016;132–133:485–90. https://doi.org/10.1016/j.clay.2016.07.019.
[19] Wang J-Q, Huang Y-X, Pan Y, Mi J-X. Hydrothermal synthesis of high purity zeolite A from natural kaolin without calcination. Microporous Mesoporous Mater 2014;199:50–6. https://doi.org/10.1016/j.micromeso.2014.08.002.
[20] Belviso C, Cavalcante F, Lettino A, Fiore S. A and X-type zeolites synthesised from kaolinite at low temperature. Appl Clay Sci 2013;80–81:162–8. https://doi.org/10.1016/j.clay.2013.02.003.
[21] Pereira P, Ferreira B, Oliveira N, Nassar E, Ciuffi K, Vicente M, et al. Synthesis of zeolite a from metakaolin and its application in the adsorption of cationic dyes. Appl Sci 2018;8(4):608. https://doi.org/10.3390/app8040608.
[22] Wang P, Sun Q, Zhang Y, Cao J. Synthesis of zeolite 4A from kaolin and its adsorption equilibrium of carbon dioxide. Materials (Basel) 2019;12(9). https://doi.org/10.3390/ma12091536.
[23] Brunauer S, Emmett PH, Teller E. Adsorption of gases in multimolecular layers. J Am Chem Soc 1938;60:309–19.
[24] Dudnikova YN, Yu Zykov I, Sozinov SA, Ismagilov ZR. Determination of the parameters of the porous structure of carbon sorbents based on Kuzbass fossil coals by the method of low-temperature nitrogen adsorption. J Phys: Conf Series, v. 1749 012020, 2021. 10.1088/1742-6596/1749/1/012020.
[25] Dubinin MM, Radushkevich LV. The equation of the characteristic curve of activated charcoal. Doklady Akademii Nauk USSR (Proceedings of the Russian Academy of Sciences) 1947;55:327–9.
[26] Toth J. State equation of the solid-gas interface layers. Act Chim Hung 1971;39:311–20.
[27] Zamani F, Rezapour M, Kianpour S. Immobilization of L-lysine on zeolite 4A as an organic-inorganic composite basic catalyst for synthesis of α, β-unsaturated carbonyl compounds under mild conditions. Bull Korean Chem Soc 2013;34. https://doi.org/10.5012/BKCS.2013.34.8.2367.
[28] Cui Y, Zheng Y, Wang W. Synthesis of 4A zeolite from kaolinite-type pyrite flotation tailings (KPFT). Minerals 2018;8(8):338. https://doi.org/10.3390/min8080338.
[29] Farmer VC. Transverse and longitudinal crystal modes associated with OH stretching vibrations in single crystals of kaolinite and dickite. Spectrochim Acta Part A Mol Biomol Spectrosc 2000;56(5):927–30. https://doi.org/10.1016/S1386-1425(99)00182-1.
[30] Madejová J. FTIR techniques in clay mineral studies. Vib Spectrosc 2003;31(1):1–10. https://doi.org/10.1016/S0924-2031(02)00065-6.
[31] Franco F, Cecila JA, Pérez-Maqueda LA, Pérez-Rodríguez JL, Gomes CSF. Particle-size reduction of dickite by ultrasound treatments: Effect on the structure, shape and particle-size distribution. Appl Clay Sci 2007;35(1):119–27. https://doi.org/10.1016/j.clay.2006.07.004.
[32] Gasparini E, Tarantino SC, Ghigna P, Riccardi MP, Cedillo-González EI, Siligardi C, et al. Thermal dehydroxylation of kaolinite under isothermal conditions. Appl Clay Sci 2013;80-81:417–25. https://doi.org/10.1016/j.clay.2013.07.017.
[33] Markovic S, Dondur V, Dimitrijevic R. FTIR spectroscopy of framework aluminosilicate structures: carnegieite and pure sodium nepheline. J Mol Struct 2003;654(1–3):223–34. https://doi.org/10.1016/s0022-2860(03)00249-7.
[34] Hayashi S, Ueda T, Hayamizu K, Akiba E. NMR study of kaolinite. 1. Silicon-29, aluminum-27, and proton spectra. J Phys Chem 1992;96(26):10922–8. https://doi.org/10.1021/j100205a058.
[35] Yao G, Lei J, Zhang X, Sun Z, Zheng S, Komarneni S. Mechanism of zeolite X crystallization from diatomite. Mater Res Bull 2018;107:132–8. https://doi.org/10.1016/j.materresbull.2018.07.021.
[36] Su S, Ma H, Chuan X. Hydrothermal synthesis of zeolite A from K-feldspar and its crystallization mechanism. Adv Powder Technol 2016;27(1):139–44. https://doi.org/10.1016/j.apt.2015.11.011.
[37] Huo Z, Xu X, Lü Z, Song J, He M, Li Z, et al. Synthesis of zeolite NaP with controllable morphologies. Microporous Mesoporous Mater 2012;158:137–40. https://doi.org/10.1016/j.micromeso.2012.03.026.
[38] Rocha J, Klinowski J. Solid-state NMR studies of the structure and reactivity of metakaolinite. Angew Chem Int Ed Engl 1990;29(5):553–4. https://doi.org/10.1002/anie.199005531.
[39] Feng W, Wan Z, Daniels J, Li Z, Xiao G, Yu J, et al. Synthesis of high quality zeolites from coal fly ash: mobility of hazardous elements and environmental applications. J Cleaner Prod 2018;202:390–400. https://doi.org/10.1016/j.jclepro.2018.08.140.
[40] Liu L, Singh R, Xiao P, Webley PA, Zhai Y. Zeolite synthesis from waste fly ash and its application in CO_2 capture from flue gas streams. Adsorption 2011;17(5):795–800. https://doi.org/10.1007/s10450-011-9332-8.
[41] Duan A, Wan G, Zhang Y, Zhao Z, Jiang G, Liu J. Optimal synthesis of micro/mesoporous beta zeolite from kaolin clay and catalytic performance for hydrodesulfurization of diesel. Catal Today 2011;175(1):485–93. https://doi.org/10.1016/j.cattod.2011.03.044.
[42] Thommes M, Kaneko K, Neimark AV, Olivier JP, Rodriguez-Reinoso F, Rouquerol J, Sing KSW. Physisorption of gases, with special reference to the evaluation of surface area and pore size distribution (IUPAC Technical Report). Pure Appl Chem, 87(9-10), 2015. doi:10.1515/pac-2014-1117.
[43] Villarreal A, Garbarino G, Riani P, Finocchio E, Bosio B, Ramírez J, et al. Adsorption and separation of CO_2 from N_2-rich gas on zeolites: Na-X faujasite vs Na-mordenite. J CO_2 Utiliz 2017;19:266–75. https://doi.org/10.1016/j.jcou.2017.03.021.
[44] Bonelli B, Civalleri B, Fubini B, Ugliengo P, Areán CO, Garrone E. Experimental and quantum chemical studies on the adsorption of carbon dioxide on alkali-metal-exchanged ZSM-5 zeolites. J Phys Chem B 2000;104(47):10978–88. https://doi.org/10.1021/jp000555g.
[45] Montanari T, Busca G. On the mechanism of adsorption and separation of CO_2 on LTA zeolites: an IR investigation. Vib Spectrosc 2008;46(1):45–51. https://doi.org/10.1016/j.vibspec.2007.09.001.
[46] Polisi M, Grand J, Arletti R, Barrier N, Komaty S, Zaarour M, et al. CO2 Adsorption/desorption in FAU zeolite nanocrystals. In situ synchrotron X-ray powder diffraction and in situ FTIR spectroscopic study. J Phys Chem C, Am Chem Soc 2019;123(4):2361–9. https://doi.org/10.1021/acs.jpcc.8b11811.
[47] Chakarova K, Andonova S, Dimitrov L, Hadjiivanov K. FTIR study of CO and N_2 adsorption on [Ge]FAU zeolites in their Na- and H-forms. Microporous Mesoporous Mater 2016;220:188–97. https://doi.org/10.1016/j.micromeso.2015.09.002.
[48] Li G, Xiao P, Webley PA, Zhang J, Singh R. Competition of CO_2/H_2O in adsorption based CO_2 capture. Energy Procedia 2009;1:1123–30. https://doi.org/10.1016/j.egypro.2009.01.148.
[49] Joos L, Swisher JA, Smit B. Molecular simulation study of the competitive adsorption of H_2O and CO_2 in zeolite 13X. Langmuir 2013;29(51):15936–42. https://doi.org/10.1021/la403824g.